UDC 666.9 : 662.613.136 : 53.091

DOI: 10.15372/CSD20180406

Hydration of Mechanically Activated Low-Lime Ash from the Thermal Power Station*

A. M. KALINKIN, B. I. GUREVICH, E. V. KALINKINA, O. A. ZALKIND

Tananaev Institute of Chemistry and Technology of Rare Elements and Mineral Raw Materials of the Kola Science Centre, Russian Academy of Sciences, Apatity, Russia

E-mail: kalinkin@chemy.kolasc.net.ru

(Received July 16, 2018; revised July 30, 2018)

Abstract

The paper explored the effect of mechanical activation of low-lime hydro removal ash of the Apatity Thermal Power Station on its binding properties without using alkaline and other chemical agents. Mechanical activation was carried out in an AGO-2 centrifugal-planetary mill for up to 400 s. The initial and mechanically activated ash were characterised by X-ray phase analysis, IR spectroscopy, scanning electron microscopy, laser granulometry, and specific surface area measurement. Following on from the data for aqueous leaching the initial mechano-activated ash, and also IR spectroscopy and thermogravimetric analysis, it was determined that mechanical activation significantly increased ash reactivity towards water. Under normal solidification, the compressive strength of ash-based samples after 60–400 s of mechanical activation aged 7 and 28 days was 0.7–1.7 and 1.4–2.2 MPa, respectively.

Keywords: TPS hydro removal ash, mechanical activation, binding properties

INTRODUCTION

Hard waste from coal-fired thermal power plants that is usually 5–20 % of the burned fuel is presented by ash (fly ash) and slag (bottom ash), the ratio of which depends on grinding fineness of coal. Captured ash is collected in the dry state for the subsequent use or forwarded to the ash-disposal area by hydro removal in a mixture with slag. The volume of annual world production of fuel ash and slags is estimated at 750 million t, moreover, only about 25 % is utilized on average [1]. In Russia, the amount of accumulated ash and slag waste from Thermal Power Stations (TPS) is about 1.5 billion t, which is associated with significant land alienation and adverse environmental impact [2].

A lot of papers (see, for example, reviews [1, 3–7]) are devoted to various methods of the utilization of waste from thermal power plants.

The key focus of the use of ash and ash-slag mixtures is the construction industry, where they can be used as part of lime-ash cements, geopolymers (alkali-activated binders), as fine-grained aggregates of concrete, *etc.* [1, 3, 5, 8–10].

Traditionally, ashes are divided into two groups, such as high-calcium (basic, class C) with CaO content more than 10 % and low-calcium (acidic, class F) with less than 10 % of calcium oxide. Unlike acidic ashes, high-calcium ones exhibit binding properties and form cement stone both independently and in combination with acidic ashes, and also other pozzolanic additives. In order to enhance the reactivity of ashes, especially low-

* Based on the materials of the V International conference "Fundamentals of mechanochemical technologies", June 25–28, 2018, Novosibirsk, Russia

lime, mechanical activation (MA) has proved itself as an efficient instrument in geopolymer and other binding compounds [11–16]. To our knowledge, there is no information in the literature regarding the mechanical activation effect on the hydraulic activity of low-calcium ash without the use of alkaline and other chemical activators.

The objective of this research was to explore binding properties of the mechanically activated hydro removal acidic ash of the Apatity TPS using only water and ash to prepare specimens.

EXPERIMENTAL

Table 1 presents the chemical composition of Apatity TPS hydro removal ash that was used in the work. The content was determined in accordance with GOST 10538-87. The following section describes the mineral composition.

Mechanical activation of ash was carried out in the AGO-2 laboratory centrifugal-planetary mill [11] in the air with a centrifugal factor of 40*g* lasting up to 400 s. Mechanical activation conditions were used as follows: grinding bodies were steel balls with a diameter of 8 mm; the ratio of the mass of the balls to the mass of the crushed sample was 6 : 1. Mixing the original or mechanically activated fly ash and water yielded normal consistency paste, from which samples with a size of 1.41 × 1.41 × 1.41 cm were formed. They were cured in the air at a humidity of 95–100 % and a temperature of 20±2 °C. The samples were tested for compressive strength using a PGM-100MG4A press. The compressive strength for each composition was determined as the arithmetic mean for three samples.

X-ray phase analysis (XPA) was performed using Shimadzu XRD 6000 X-ray diffractometer (CuK_α radiation). Recording X-ray diffraction patterns was performed with a step of 0.02° (2θ), signal accumulation time in each point of 1 s. Thermal analysis of hardened samples was carried out using a Paulik–Paulik–Erdei derivatograph (MOM, Hungary) at a 100 °C/min heating rate. The specific surface area (S_{sp}) of powders was measured by low-temperature nitrogen adsorption using the Flow Sorb II 2300 analyser (Micromeritics) and by Blaine method. The particle size distribution was determined using SALD-201V laser diffraction particle size analyser.

The IR spectra were recorded using the Nicolet 6700 FTIR spectrometer in KBr pellets. In order to obtain images by scanning electron microscopy (SEM), an LEO-1450 microscope was used. The carbon content was determined using the ELTRA CS-2000 analyser. Ash leaching was performed with distilled water at 20±2 °C with a solid/liquid ratio of 1 : 40 using magnetic stirring for 5 h. After filtration, the liquid phase was analysed using the ICPE-9000 inductively coupled plasma atomic emission spectrometer (Shimadzu).

RESULTS AND DISCUSSION

The basis of the Apatity TPS ash (about 60 %) is the glass phase as spherical particles (microspheres), along with which ash contains sintered irregularly shaped mineral particles with a developed surface in a comparable amount [17–19]. Both types of particles are clearly visible in the SEM image of the initial ash (Fig. 1, *a*). Mechanical activation for 60 seconds leads to a significant reduction in particle size and breakage of the larger part of microspheres (see Fig. 1, *b*). After 180 s of mechanical activation, according to SEM data (not shown), almost all microspheres are destroyed.

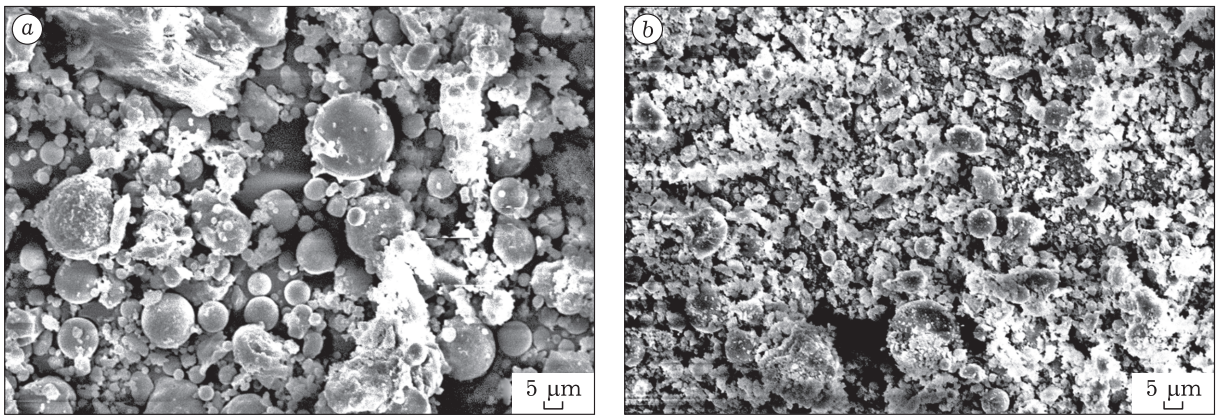

Fig. 1. SEM images of the original ash (*a*) and ash after 60 s of mechanical activation (*b*).

Figure 2 gives X-ray diffraction patterns of the initial (curve *1*) and mechanically activated ash for 400 s (curve *2*). Resulting from mechanochemical treatment in a planetary mill, there is the broadening of reflections of crystal phases that are part of ash composition, such as quartz, mullite, magnetite, and hematite due to a decrease in sizes of crystallites (coherent scattering regions) or/and microdeformation of crystalline lattices.

It was impossible to separate contributions of these two factors because of the overlapping of diffraction peaks and low intensity of a significant portion of them.

The X-ray diffraction pattern of mechanically activated ash contains a broad peak corresponding to the main reflection of elemental iron that appears in the sample resulting from the autogenous grinding of mill balls and vial (milling yield). According to chemical analysis data, the milling yield is about 1 % mass of Fe after 400 s of mechanical activation.

The IR spectrum of the initial ash (Fig. 3, curve *1*) contains bands of Si–O–Si asymmetric stretching vibrations (1165 cm^{-1}), T–O–Si asymmetric stretching vibrations, where T = Al or Si (1085 cm^{-1}), Si–O–Si symmetric stretching vibrations (797 and 776 cm^{-1}), T–O–Si symmetric stretching vibrations , where T = Al or Si (692 cm^{-1}), symmetric stretching vibrations of Al–O–Si (557 cm^{-1}), and Si–O–Si deformation vibrations (460 cm^{-1}).

In agreement with XRF data (see Fig. 2), the shoulder at 1165 cm^{-1} and bands at 1085, 797, 776, 692, and 460 cm^{-1} correspond to α-quartz, and the band at 557 cm^{-1} is corresponding to mullite [9, 20]. The broad band at 1085 cm^{-1} may also be referred to the amorphous aluminosilicate phase of ash [9]. The bands at 3430 and 1630 cm^{-1}, respectively, correspond to the stretching and bending vibrations of water adsorbed on the surface of ash particles. The band at 1418 cm^{-1} corresponds to symmetrical bending vibrations of the CO_3^{2-} group in the composition of carbonates formed during the interaction of ash and atmospheric carbon dioxide.

Mechanical activation of ash for 400 s leads to a notable increase in the intensity of adsorption bands in the 1100–400 cm^{-1} range, especially the band of Si(Al)–O–Si asymmetric stretching vibrations near 1085 cm^{-1} (see Fig. 3, curve *2*). Similar changes in IR spectra of mechanically activated ash noted earlier in [14, 21] may be probably related to rearrangements in the nearest atoms surrounding. There is also an increase in the intensity

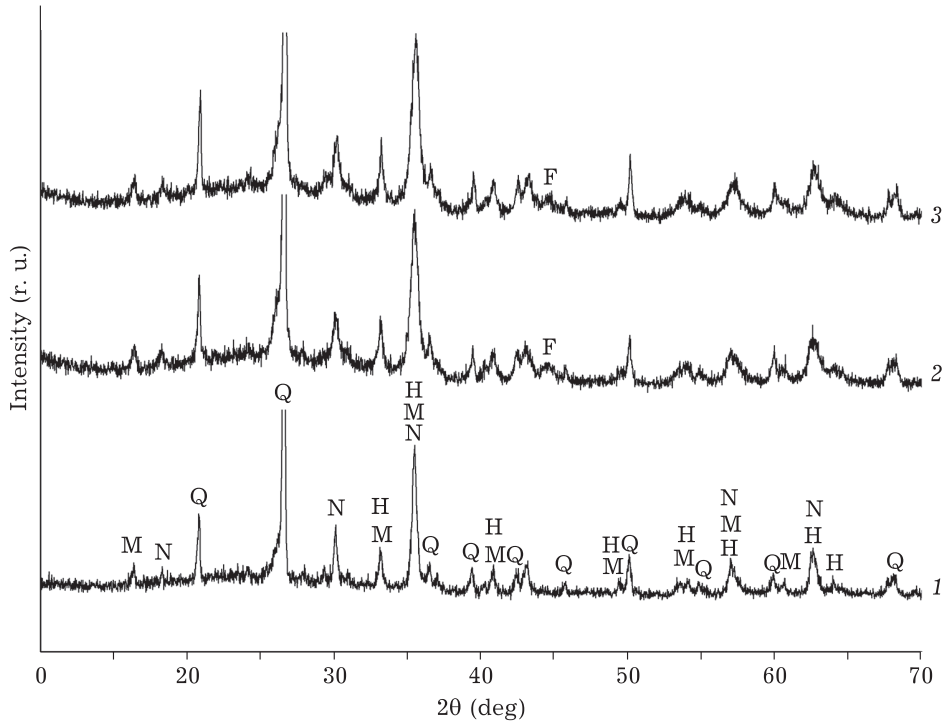

Fig. 2. X-ray diffraction patterns of the initial ash (*1*), ash after 400 s of mechanical activation (*2*) and a sample based on ash mechanically activated for 400 s, after curing for 28 days (*3*). Solid phases: Q – α-quartz SiO_2 (PDF 46-1045), M – mullite $3Al_2O_3 \cdot 2SiO_2$ (PDF 15-776), N – magnetite Fe_3O_4 (PDF 19-629), H – hematite Fe_2O_3 (PDF 33-664), F – elemental iron (PDF 6-696).

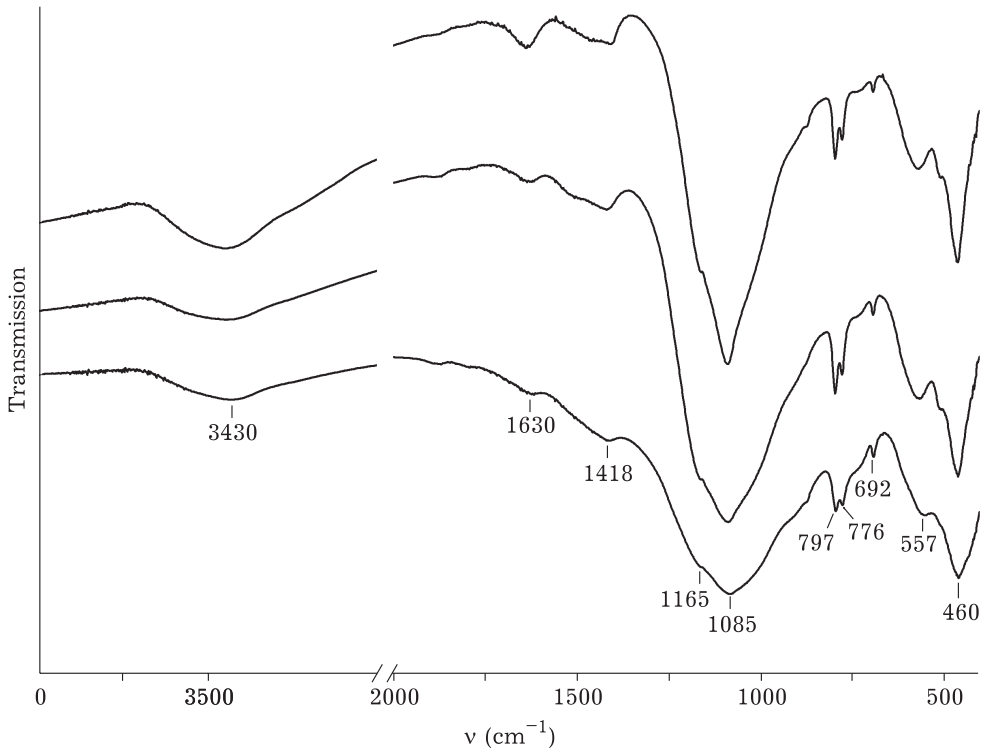

Fig. 3. IR spectra of the initial ash (*1*), ash after 400 s of mechanical activation (*2*) and a sample based on ash mechanically activated for 400 s, after curing for 28 days (*3*).

and the broadening of the carbonate band in the 1500–1400 cm^{-1} range, which may be explained by mechanically induced sorption of atmospheric carbon dioxide as CO_3^{2-} groups due to the presence of alkaline earth metals in ash [22]. The results of chemical analysis of the initial ash and ash after 400 s of mechanical activation prove this conclusion. According to the analysis, carbon content therein was 0.89±0.02 and 1.38±0.03 % of carbon, respectively. It is worth noting that these values characterize the total carbon content, both carbonate and that in the composition of the unburned residue of coal fuel (underburning).

Figure 4 gives the specific surface area of ash versus mechanical activation time. According to the data acquired by Blaine method, the maximum specific surface area is reached after 250–300 s of mechanical activation; afterwards, S_{sp} is gradually reduced (see Fig. 4, curve *1*). Alongside with that, the specific surface area determined according to nitrogen low-temperature adsorption increases steadily in the whole range of mechanical activation time (see Fig. 4, curve *2*). This testifies that the internal surface of aggregates is accessible for gas molecules.

Figure 5 presents integral particle-size distribution curves for initial and mechanically activated ash. The same figure gives indicators d_{25}, d_{50}, and d_{75} values. In accordance with the data for S_{sp} (see Fig. 4), the most intense disintegration of ash proceeds within the first 180 s of mechanical activation. In particular, the median diameter, d_{50} decreases from 17.3 μm for the initial ash to 3.33 μm for mechanically activated one for 180 s, *i.e.* by more than 5 times. During the next 220 s (mechanical activation total time of 400 s), d_{50} is reduced as high as 2.79 μm, *i.e.* by 1.2 times with against the sample after 180 s of mechanical activation.

Figure 6 presents compressive strength data for samples based on initial and mechanically activated ash after curing at normal conditions for 7 and 28 days. With increasing mechanical treatment time, the strength continuously increases, reaching 1.7 and 2.2 MPa for ash-based samples after 400 s of mechanical activation aged 7 and 28 days, respectively. It is also worth noting that the initial ash has insignificant binding properties, in other words, the strength was 0.3 MPa after 28 days of curing at normal conditions (Fig. 6, curve *2*). There was no positive effect of iron impurity in ash on strength because of milling. The destructive effect of milling in the course of hardening aluminosilicate geopolymer composite was found in [23]. The effect is due to the fact that during hydration, goethite FeO(OH) is formed re-

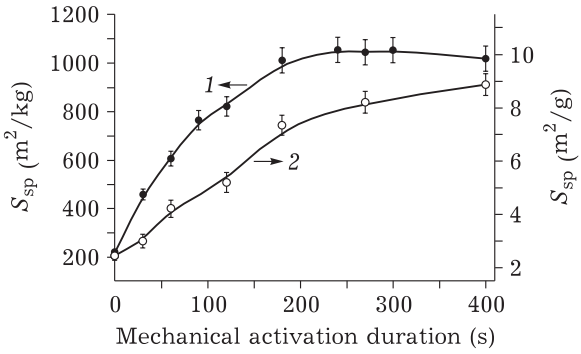

Fig. 4. Dependence curves of the ash specific surface area measured by Blaine method (*1*) and low-temperature nitrogen adsorption (*2*) versus mechanical activation duration.

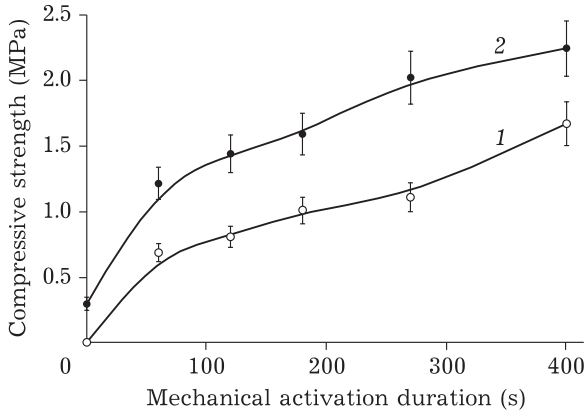

Fig. 6. Compressive strength of ash samples after curing at normal conditions for 7 (*1*) and 28 days (*2*) depending on mechanical activation duration.

sulting from milling yield; its volume is 3 times higher than that of the metal iron. This causes the appearance of cracks in the samples and a drop in strength. Therefore, having reduced milling yield, for example, by having used the method of self-lining [24] or using a more wear-resistant material of the balls and the grinding vial, one may expect improved binding properties of mechanically activated ash.

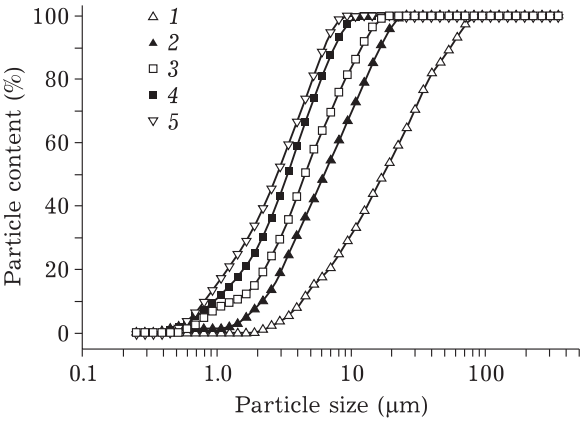

Fig. 5. Integral curves of ash particles size distribution: *1* – initial ash; *2–5* – after 30, 120, 180, and 400 s of mechanical activation, respectively.

Upper boundaries of particle diameters (μm), contents of which are 25 (d_{25}), 50 (d_{50}), and 75 % (d_{75})

Curve No.	d_{25}	d_{50}	d_{75}
1	8.11	17.3	33.1
2	3.42	6.28	11.4
3	2.59	4.47	7.91
4	1.88	3.33	5.33
5	1.43	2.79	4.63

As noted above, in order to explore strength properties, small-sized samples (1.41 × 1.41 × 1.41) cm were used. Having determined the corresponding conversion factors, the resulting strength may be recalculated into strength according to GOST samples.

Table 1 gives solutions analysis results and the extraction degree of the main components of initial and mechanically activated ash into the liquid phase during aqueous treatment.

Following on from the research on the interaction of a broad range of aluminosilicate minerals with solutions of alkali metal hydroxides, it was demonstrated in [25] that in geopolymer synthesis, it was relatively hard to reveal unambiguous correlations between extraction of components into the liquid phase and geopolymers strength. Using factor analysis method, it was found that among all the main elements contained in aluminosilicates, silicon leaching into a solution was of the greatest importance against increasing geopolymer strength. In our experiments, ash treatment was carried out with water rather than with alkaline solutions. Nevertheless, as it follows from the data in Table 1, a rise in strength with increasing mechanical activation time (see Fig. 6) also agrees best with the corresponding enhanced extraction of silicon into the liquid phase.

It is known that an increase in the reactivity of solids during mechanical activation is driven by not only and not so much increasing S_{sp} resulting from disintegration. The accumulation of dislocations and other defects in a solid has a significantly larger impact on the rate of heterogeneous processes with the involvement of mechanically activated powders. As a result, if there are no diffusion limitation and side processes, the

TABLE 1
Concentrations of Al_2O_3, SiO_2, MgO, CaO, and Fe_2O_3 in the liquid phase after aqueous leaching of initial and mechanically activated ash, mg/L

Component	Duration of MA, s		
	0	180	400
Al_2O_3	1.04 (0.027 %)	1.23 (0.032 %)	1.33 (0.034 %)
SiO_2	3.85 (0.039 %)	6.59 (0.067 %)	6.76 (0.070 %)
MgO	11.2 (1.68 %)	13.3 (2.00 %)	13.8 (2.07 %)
CaO	39.2 (5.34 %)	43.0 (5.85 %)	42.0 (5.72 %)
Fe_2O_3	0.39 (0.01 %)	0.40 (0.01 %)	0.39 (0.01 %)

Note. Values of recovery degree of components computed according to their solution concentrations and contents in ash are given in brackets.

rate of dissolution of mechanically activated substances increases faster than the specific surface area does [26, 27]. The indicated trend is not adhered for the aqueous treatment of ash, which testifies a more complex nature of the interaction. For example, ash specific surface area measured according to the nitrogen low-temperature adsorption method after 400 s of mechanical activation is by 3.6 times higher than a similar value for the initial ash (see Fig. 4). Alongside with that, extraction of silicon, aluminium, and magnesium into a solution after mechanical activation of ash for 400 s is increased by 1.8, 1.3, and 1.2 times, respectively, while for calcium and iron, the leaching into the liquid phase almost does not depend on mechanical activation time and specific surface area (see Table 2). It is noteworthy that the degree of leaching of calcium and magnesium is by 2 orders of magnitude higher than a similar value for silicon and aluminium (see Table 2). Apparently, such a low extraction of Si and Al is related to their precipitation as hydrated silica (silica gel) and low-soluble amorphous hydro-aluminosilicates [28, 29].

The data of IR spectroscopy and thermal analysis prove the hydration of mechanically activated ash. The IR spectrum of a sample based on 28 day-aged ash mechanically activated for 400 s (see Fig. 3, curve *3*) has a significant narrowing of the band of Si(Al)–O–Si asymmetric stretching vibrations in the 1200–1000 cm^{-1} range. This testifies the appearance of cementitious newly formed phase with a more ordered location of Si(Al) oxygen tetrahedra. The cementitious phase is of amorphous nature, as there are no new reflections in X-ray diffraction patterns of hardened samples compared to mechanically activated ash (see Fig. 2, curves *2* and *3*).

There was a similar decrease in the width of the band of Si–O–Si asymmetric stretching vibrations during hardening of mechanically activated hydrated magnesia ferriferous slag, the basis of which was glass of the olivine composition [30].

According to thermogravimetric analysis data (not given), the correlations of the strength of samples with mass losses have been found in the 120–320 °C range. The latter are likely related to the dehydration of newly formed hydrosilicates. For instance, the mass loss for 28 day-aged ash-based samples prepared using ash after 180 and 400 s of mechanical activation (compressive strength of 1.6 and 2.2 MPa, respectively) was 1.1 and 1.8 %, respectively.

CONCLUSIONS

1. Resulting from mechanical treatment of low-lime hydro removal ash of the Apatity TPS in a centrifugal-planetary mill, there is an increase in the intensity of Si(Al)–O–Si stretching vibrations near 1200–1000 cm^{-1} in the IR spectrum. This is probably driven by rearrangements in the nearest atoms surrounding. According to IR spectroscopy and chemical analysis data, mechanical activation of ash for 400 s results in absorption of atmospheric carbon dioxide in the form of carbonate groups (about 0.5 mass % per carbon).

2. There is the most intense increase in the specific surface area of ash within the first 180 s of mechanical activation. The ash specific surface area determined by the Blaine method passes through a gentle maximum in the range of 250–300 s of mechanical activation and then gradually decreases due to the enhanced formation of aggregates, the inner surface of which is accessible for nitrogen molecules.

3. Mechanical activation of ash markedly increases its reactivity towards the water. As a consequence, unlike the initial ash, mechanically activated one exhibits hydraulic properties without the use of chemicals. For example, under curing at normal conditions, the compressive strength of 28 day-aged ash-based samples prepared using ash after 60–400 s of mechanical activation is 1.4–2.2 MPa.

4. Experimental data on the aqueous leaching of ash, and also IR spectroscopy and X-ray phase analysis for hardened samples make it possible to assume that the cementitious phase is formed resulting from the intensification of the transition of silicon and other components of mechanically

activated ash into the liquid phase followed by the formation of silica gel and X-ray amorphous hydro-aluminosilicates.

Acknowledgements

The authors thank V. V. Semushin for ash analysis by scanning electron microscopy.

REFERENCES

1 Yao Z. T., Ji X. S., Sarker P. K., Tang J. H., Ge L. Q, Xia M. S., Xi Y. Q., *Earth-Science Reviews*, 2015, Vol. 141, P. 105–121.
2 Delitsyn L. M., Ezhova N. N., Vlasov A. S., Sudareva S. V., *Journal of Industrial Ecology*, 2012, Issue 4, P. 15–26 (in Russ.).
3 Blissett R. S., Rowson N. A., *Fuel*, 2012, Vol. 97, P. 1–23.
4 Lee Y.-R., Soe J. T., Zhang S., Ahn J.-W., Park M. B., Ahn W.-S., *Chem. Eng. J.*, 2017, Vol. 317, P. 821–843.
5 Ahmaruzzaman M., *Prog. Energy Combust. Sci.*, 2010, Vol. 36, P. 327–363.
6 Ding J., Ma S., Shen S., Xie Z., Zheng S., Zhang Y., *Waste Manag.*, 2017, Vol. 60, P. 375–387.
7 Bukhari S. S., Behin J., Hossein Kazemian H., Rohani S., *Fuel*, 2015, Vol. 140, P. 250–266.
8 Entin Z. B., Nefedova L. S., Strzhalkovskaya N. V., *Cement and Its Application*, 2012, Issue 2, P. 40–46 (in Russ.).
9 Lee W. K. W., van Deventer J. S. J., *Colloids and Surfaces A: Physicochem. Eng. Aspects.*, 2002, Vol. 211, P. 49–66.
10 Alkali Activated Materials, State-of-the-Art Report. RILEM TC 224-AAM, J. L. Provis, J. S. J. van Deventer (Eds.) London: Springer, 2014. 388 p.
11 Avvakumov E. G., Gusev A. A., Mechanical Methods of Activation in the Processing of Natural and Technogenic Raw Materials, Novosibirsk: Geo, 2009. 155 p. (in Russ.).
12 Lomovskiy O. I., Boldyrev V. V., Mechanochemistry for Solving Environmental Problems, Novosibirsk: GPNTB Siberian Branch of the Russian Academy of Sciences, 2006. 221 p. (in Russ.).
13 Mucsi G., J. *Silicon Based Compos. Mater.*, 2016, Vol. 68, No. 2, P. 56–61.
14 Kumar R., Kumar S., Mehrotra S. P., *Resour. Conserv. Recycl.*, 2007, Vol. 52, P. 157–179.
15 Tchadjie L. N., Ekolu S. O., *J. Mater. Sci.*, 2018, Vol. 53, P. 4709–4733.
16 Shoeva T. E., Kaminskiy Yu. D., *Natural and Technical Sciences*, 2009, Issue 1, P. 376–379 (in Russ.).
17 Tyukavkina V. V., Brylyakov Yu. E., Gurevich B. I., *Cement and Its Application*, 2017, Issue 5, P. 78-80 (in Russ.).
18 Pak A. A., Sukhorukova R. N., Polistirolgazobeton: Technology and Properties of Composite Products, Apatity: Publishing of the Kola Science Centre of the Russian Academy of Sciences, 2012. 101 p. (in Russ.).
19 Kozhukhova N. I., Zhernovskiy I. V., Fomina E. V., *Construction Materials*, 2015, Issue 12, P. 85–88 (in Russ.).
20 Fernandez-Jimenez A., Palomo A., *Microp. Mesop. Mater.*, 2005, Vol. 86, P. 207–214.
21 Kumar S., Kumar R., *Ceram. Int.*, 2011, Vol. 37, P. 533–541.
22 Kalinkin A. M., Kalinkina E. V., Politov A. A., Makarov V. N., Boldyrev V. V., *J. Mater. Sci.*, 2004, Vol. 39, No. 16–17, P. 5393–5398.
23 Kozhukhova N. I., Strokova V. V., Chizhov R. V., Geopolymer Binder and Fine-grained Concrete Based on Perlite, Belgorod: Publishing of the V. G. Shukhov Belgorod State Technological University, 2017. 130 p. (in Russ.).
24 USSR Inventor's Certificate No. 1375328, 1988.
25 Xu H., van Deventer J. S. J., *Int. J. Miner. Process.*, 2000, Vol. 59, P. 247–266.
26 Khodakov G. S., Physics of Grinding, Nauka: Moscow, Russia, 1972. p. 307. (in Russ.).
27 Eremin A. F., Gol'dberg E. L., *Izvestiya of the Siberian Branch of the Academy of Sciences of the USSR. Series of Chemical Sciences*, 1985, Vol. 17, Issue 6, P. 12–16 (in Russ.).
28 Butt Yu. M., Rashkovich L. N., Hardening of Binders at Elevated Temperatures, Moscow: Publishing House of Literature on Construction, 1965. 223 p. (in Russ.).
29 Kim A. G., Hesbach P., *Fuel.*, 2009, Vol. 88, P. 926–937.
30 Kalinkin A. M., Gurevich B. I., Myshenkov M. S., Kalinkina E. V., Zvereva I. A., *J. Therm. Anal. Calorim.*, 2018. URL: https://doi.org/10.1007/s10973-018-7439-9 (accessed 30.07.18).